Atmospheric forcing of Fram Strait sea ice export:

A closer look

Maria Tsukernik[1]

Clara Deser[1]

Michael Alexander[2]

Robert Tomas[1]

[1] National Center for Atmospheric Research

[2] NOAA Earth System Research Laboratory

Submitted to Climate Dynamics,

March 16, 2009

Corresponding author: Maria Tsukernik, Climate and Global Dynamics Division, NCAR, P.O. Box 3000, Boulder, CO 80307, masha@ucar.edu

Abstract

Fram Strait is the primary region of sea ice export from the Arctic and therefore plays an important role in regulating the amount of sea ice and freshwater within the Arctic. We investigate the variability of Fram Strait sea ice motion and the role of atmospheric circulation forcing using daily data during the period 1979-2006. The most prominent atmospheric driver of anomalous sea ice motion across Fram Strait is an east-west dipole pattern of Sea Level Pressure (SLP) anomalies with centers-of-action located over the Barents Sea and Greenland. This pattern, also observed in synoptic studies, is associated with anomalous meridional winds across Fram Strait and is thus physically consistent with forcing changes in sea ice motion. The association between the SLP dipole pattern and Fram Strait ice motion is maximized at 0-lag, persists year-round, and is strongest on time scales of 10-60 days. The SLP dipole pattern is the 2nd Empirical Orthogonal Function (EOF) of daily SLP anomalies in both winter and summer.

When the analysis is repeated with monthly data, only the Barents center of the SLP dipole remains significantly correlated with Fram Strait sea ice motion. However, after removing the leading EOF of monthly SLP variability (e.g. the North Atlantic Oscillation), the full east-west dipole pattern is recovered. No significant SLP forcing of Fram Strait ice motion is found in summer using monthly data, even when the leading EOF is removed. Our results highlight the importance of high frequency atmospheric variability in forcing Fram Strait sea ice motion.

1. Introduction

Fram Strait, located between Greenland and Svalbard, is the primary gateway for the export of sea ice out of the Arctic (Kwok, et al. 2004). Fram Strait sea ice export is highly variable from day to day and from year to year (Vinje, 2001, Brummer et al. 2001 and 2003). Such high variability affects other components of the Arctic climate system: for example, anomalous Fram Strait export has been linked to the "Great Salinity Anomaly" in the North Atlantic (Dickson et al., 1988) and to the recent decline of summer sea ice extent (Rigor and Wallace, 2004).

The relationship between the large-scale patterns of atmospheric variability especially the North Atlantic Oscillation (NAO; Hurrell, 1995) and the related Arctic Oscillation (AO; Thompson and Wallace, 1998) with sea ice export through Fram Strait has been investigated in numerous studies, for example: Kwok and Rothrock, 1999; Hilmer and Jung, 2000; Jung and Hilmer, 2001; Vinje 2001; Rigor et al., 2002; Kwok et al., 2004. During the last two decades of the 20th century (e.g. 1978-1997) the correlation between the NAO and sea ice export through Fram Strait was highly positive (e.g. Hilmer and Jung, 2000, Kwok et al. 2004); however, the correlation during other time periods (e.g. 1958-1977) was near zero or even slightly negative (Hilmer and Jung, 2000, Vinje 2001, Jung and Hilmer, 2001).

Given the ambiguity in the relationship between the NAO/AO and Fram Strait sea ice export, Wu et al. (2006 and 2007) investigated whether other patterns of atmospheric variability are related to the ice export in winter. Wu et al. (2006) identified an east-west dipole pattern with centers of action over the Kara/Laptev Seas and the Canadian Archipelago to be an important forcing for sea ice export through Fram Strait,

while Wu et al. (2007) argued that another pattern with a center of action over the Barents Sea plays even a bigger role in forcing Fram Strait sea ice export. Maslanik et al. (2007) indicated that the strength and position of the centers of action of atmospheric circulation variability associated with sea ice motion within the Arctic basin are affected by cyclone frequency and strength, and that both factors vary considerably from year to year.

To examine the link between sea ice export and atmospheric circulation patterns in more detail, Brummer et al. (2003) analyzed how a single cyclone passing through Fram Strait influences sea ice motion. They found that ice velocity increased by a factor of three during the passage of the cyclone, and that the ratio of ice drift to wind speed also increased. Brummer et al. (2001) analyzed 16 years of cyclone statistics from ERA-40 and corresponding sea ice drift observations. They found that sea ice motion is quite sensitive to the particular cyclone trajectory and concluded that, on average, cyclones increase sea ice export through Fram Strait. Rogers et al. (2005) investigated the role of winter cyclones in Fram Strait sea ice export and found a correspondence between increased cyclogenesis along the northeast coast of Greenland and low sea ice export. High sea ice export years, on the other hand, corresponded to the persistent cyclones in the Norwegian and Barents Seas. Using a case study approach, Tsukernik (2007) illustrated how a particular cyclone trajectory influences sea ice motion: a cyclone passing through Fram Strait can completely reverse the direction of sea ice export, while a cyclone passing east of Fram Strait dramatically increases the sea ice export.

Although the topic of atmospheric influence on Fram Strait sea ice export has received a lot of attention, there is still a gap between the monthly-averaged studies that relate the sea ice export to large-scale atmospheric patterns and the synoptic-scale studies that investigate the role of high frequency atmospheric disturbances in sea ice export. To bridge this gap, we use daily data to investigate the relationship between the atmospheric circulation and sea ice export over a range of time scales. Due to the scarcity of sea ice thickness measurements, we focus on the areal flux of sea ice through Fram Strait based on satellite estimates of sea ice motion. We investigate the spatial structure and temporal evolution of the Sea Level Pressure (SLP) patterns associated with variations in sea ice motion through Fram Strait, including its seasonal and frequency dependence. This paper is organized as follows. In Section 2 we describe the datasets and methods used in this study. In Section 3 we present main results, and in Section 4 we summarize our results and discuss them along with findings from previous research.

2. Data and methods

We use 6-hourly NCEP/NCAR Reanalysis (Kalnay et al., 1996) SLP and daily sea ice motion vectors from the 25 km Polar Pathfinder product available from the National Snow and Ice Data Center (Fowler, 2003) during 1979-2006. Since we are interested in Fram Strait sea ice export, we derive an index of the meridional component of sea ice motion averaged across the Strait (20°W - 15°E, 79° - 81°N; region in red outlined in Figure 1). A negative sea ice index indicates northward ice motion, while a

positive sea ice index indicates southward ice motion across Fram Strait. We smooth the 6-hourly NCEP SLP data using a running five-point centered average to produce daily averages that match the resolution of the sea ice index. To define daily anomalies we remove the first two harmonics of the seasonal cycle from both the sea ice index and the gridded SLP time series.

We use linear correlation and regression analysis to define anomalous SLP conditions associated with changes in sea ice export. The statistical significance of the correlation and regression values is assessed using a 2-sided student t-test, taking into account the autocorrelation of both series (Press et al., 1986). In order to investigate the relationship between the atmospheric circulation and sea ice export on different timescales we perform cross-spectrum analysis (Julian, 1975; Bloomfield, 1976). Based on the cross-spectrum results, we define a band pass filter with half-power points at 10 and 60 days (Dunchon, 1979).

To investigate the seasonal dependence of the sea ice – atmosphere relationship, we divide record into two seasons: winter (October 15 to April 14) and summer (April 15 to October 14). We subsequently apply all of the techniques described above to the two seasons separately. As the cross-spectrum can only be calculated for a continuous time period, we calculate the spectrum for each winter and summer during 1979-2006 separately and then average individual power spectra together.

3. Results

a. Daily data

Figure 1 depicts the correlation coefficient map between SLP north of 40°N and the Fram Strait sea ice motion index based on 10,227 days of data during 1979-2006. Due to the large sample size, correlation coefficients exceeding ~0.05 in absolute value are statistically significant at the 99% level (outlined by white contour in Figure 1). There are two main centers of action associated with the anomalous sea ice motion: one over Barents Sea and another one over northern Greenland and Canadian Archipelago. As the sign of the correlation coefficients suggest, southward Fram Strait sea ice motion is maximized with a Barents Sea Low and a Greenland High. Such an east-west dipole pattern is associated with geostrophic northerly winds in Fram Strait and therefore is physically consistent with increased sea ice transport. As previous studies have indicated, sea ice in the Arctic Ocean moves nearly parallel to the geostrophic wind (Thorndike and Colony, 1982; Kimura and Wakatsuchi, 2000).

An analogous SLP pattern has been described in the literature related to the cold-air outbreaks in Scandinavia (Kolstad et al., 2008). A similar east-west dipole pattern emerges as the second empirical orthogonal function (EOF) of the daily SLP anomalies over the Atlantic sector (90ºW-90ºE, 45º-90ºN) during 1979-2006 and explains 14% of the variance; while the leading EOF resembles the North Atlantic Oscillation (NAO; Hurrell 1995) and accounts for 32% of the variance (Figure 2). Previous studies have also obtained a dipole pattern from EOF analysis based on

monthly SLP anomalies (e.g."Barents Oscillation" described by Skeie 2000 and Tremblay 2001; winter dipole pattern described by Wu et al. 2006).

We employ the two centers of action revealed by the correlation coefficient map (Figure 1) to construct a SLP gradient index (SLPGI). For simplicity we define the centers as square boxes, both outlined in Figure 1. The Barents center of action stretches from 72.5° to 77.5°N and from 17.5° to 50.0°E, and the Greenland center of action occupies the area from 75.0° to 80.0°N and from 60.0° to 42.5°W. We define a SLPGI as the difference between these two centers of action. Our results are not sensitive to the exact definition of the Barents and Greenland centers of action – bigger and smaller square boxes defining the SLPGI provide similar results (not shown).

The standardized time series of the SLPGI and Fram Strait sea ice motion index for one particular winter season (1985-1986) are presented in Figure 3. The winter of 1985-86 is chosen for illustration only but it is fairly representative of the entire record. The SLPGI and ice motion index exhibit similar behavior, with an overall correlation coefficient of 0.54, significant at the 99% level. Both time series experience substantial high frequency (sub-monthly) variability and therefore monthly averages cannot sufficiently describe these variables. Peaks and troughs of the SLPGI and ice motion time series often occur simultaneously, with no systematic lead or lag between the two. There are, however, short periods of non-simultaneous change (for example the second half of November 1985), which is expected from noisy high resolution indices.

Figure 4 depicts the anomalous SLP pattern associated with enhanced southward sea ice motion through Fram Strait, obtained by regressing the daily SLP

anomaly time series at each grid point upon the daily ice motion anomaly time series. The top panel shows results based on all 10,227 days in the 1979-2006 record; the middle and lower panels depict results based on the winter (October 15 to April 14) and summer (April 15 to October 14) seasons of the year. The SLP regression coefficients are in the units of hPa per cm s^{-1} and are thus representative of a 1 cm s^{-1} increase in the southward ice motion through Fram Strait. Overall, the seasonal variations are quite small: both the Greenland and Barents centers of action persist year-round, although they are ~15% stronger (and the Barents center is also more extensive) in winter compared to summer. Thus, the same ice motion anomaly is associated with a stronger geostrophic northerly wind anomaly in winter than summer. Considering that sea ice in winter is generally thicker, more compact and harder to move than in summer (e.g. Kwok et al. 2004), these differences are not surprising.

Due to the persistence of the east-west dipole pattern year-round, we define the SLPGI for winters and summers based on the same two centers of action (see Figure 1). The lead/lag correlation and regression coefficients between Fram Strait sea ice motion index and the SLPGI for all days of the year, and for winter and summer separately are presented in Figure 5. Both maxima of correlation and regression values occur at zero lag and both decline sharply to ~20% of their maximum values (e.g. approximate e-folding time) at +/- 5 days. Such a sharp decline suggests a lack of inertia in the wind – sea ice relationship, a rather surprising finding. Simultaneous correlation (regression) coefficient values range from 0.58 (1.33 hPa cm^{-1} s) in winter to 0.49 (1.12 hPa cm^{-1} s) in summer, consistent with the values in Figures 1 and 4. Values exceeding 0.04 (0.12 hPa cm^{-1} s) are significant at the 99% level. Winter values also

exhibit greater inertia than summer, as evidenced by small positive correlation values at lags of 8-15 days.

The daily data used in this study allow us to investigate the spectral character of the relationship between the SLPGI and Fram Strait sea ice motion index in detail. Figure 6 depicts the coherence between the two variables, which is equivalent to the correlation coefficient as a function of frequency. Coherence values are shown for periods between 2 days and 5 years; values exceeding 0.22 are significant at the 99% level (yellow line). Coherence values peak in the 10 to 60 day band, with values between 0.6 and 0.75. Coherence values are lower than 0.5 at periods shorter than 5 days and longer than 200 days. Lower coherence values for periods > ~200 days suggest factors in addition to wind forcing are important in connection with sea ice motion through Fram Strait on interannual timescales.

The seasonality of the coherence values, calculated by averaging the power spectra for each year separately, is shown in Figure 7. Note, that this method yields higher coherence values for periods shorter than ~5 days than those in Figure 6 due to the averaging procedure. It also can only resolve periods shorter than ~180 days. Both winters and summers exhibit maximum coherence values in the 10 to 60 day band, with higher coherence values in winter(0.70 - 0.75) than those in summer (0.60 - 0.70). The winter coherence curve is very similar to that based on all days of the year, except for the higher values at periods longer than 60 days.

Given that the strongest association between the SLPGI and the Fram Strait sea ice motion index occurs in the 10-60 day range, we have recomputed the SLP

regression coefficients upon the ice index using 10-60 day band pass filtered daily data. Figure 8 depicts the time evolution of the regression coefficients for the winter season from a lag of -8 days (SLP leading) to a lag of +8 days (SLP lagging). Similar patterns are obtained using year-round data (not shown). At -8 day lag (top left) there is a weakly defined dipole pattern of reversed sign, compared to that at 0 lag (Figure 4 and middle panel of Figure 8). The sign reversal is partially due to the response curve of the 10-60 day filter, while the weak amplitude of the regression values suggests a lack of inertia in the system as mentioned before. As time progresses (-6 and -4 day lags) a low SLP anomaly moves into the Barents Sea and by -2 day lag (middle left panel) the Barents and Greenland centers are well-defined with regression coefficients values increasing dramatically. The regression coefficients reach their maximum values at 0 lag, consistent with the results based on unfiltered data. The regression pattern dissipates almost as quickly as it develops. The bottom row of panels depicts the Barents low center gradually moving southeastward at +2, +4 and +6 day lags. By +8 day lag (bottom right), the regression pattern once again is weak and of reversed polarity.

Figure 9 shows the lead/lag correlation and regression coefficients between the SLPGI and Fram Strait ice motion index based on the 10-60 day band pass filtered data. As expected, the simultaneous correlation regression coefficients increase after filtering (compare Figures 5 and 8), with correlation (regression) values of 0.69 (~2 hPa cm^{-1} s) in winter and 0.64 (1.9 hPa cm^{-1} s) in summer. Both regression and coefficient values experience sharp declines beyond weekly lags. Negative values observed at periods of 1-3 weeks are likely to be an artifact of the filtering.

Because the Greenland center of action encompasses the region near Iceland (see Figure 8, middle row, -2 days to +2 days lags) and because the regression values near the Azores (40°N, 30°W) are of opposite polarity, a statistical relationship exists between the NAO-index and the sea ice motion through Fram Strait. To examine this association in more detail, we develop an NAO-like index based on the difference between the Icelandic (55°- 65°N and 40°- 10°W) and Azores centers of actions (35° - 45°N and 40°- 20°W). Note that our sign convention is opposite to the traditional definition of the NAO (Hurrell et al., 1995). The lag regression between the NAO-like index and the sea ice motion index based on unfiltered and 10-60 day filtered data for winter only are depicted by green curves in Figures 5 and 9 respectively. As evident from these figures, the NAO-like relationship with sea ice motion is much weaker than that of the SLPGI, although significant at the 99% level.

b. Monthly data

We have repeated the correlation/regression analysis using monthly averages for direct comparison to previous studies. Figure 10 (top panel) shows the simultaneous regression of monthly SLP anomalies on the monthly sea ice motion index based on all months of the year during 1979-2006. The striking feature of the monthly regression map compared to the daily regression map (Figure 4) is the disappearance of the Greenland center of action and therefore the dipole structure of the pattern. The Barents center of action is still present and statistically significant at the 99% level. Although the dipole atmospheric pattern is not present, the Barents low pressure center

still produces a SLP gradient across Fram Strait, providing the necessary forcing for the underlying sea ice.

The seasonal structure of the monthly regression map is also noticeably different from that of the daily regression map. With monthly data, the Barents center of action is active in winter only, while no significant relationship between SLP and sea ice motion exists in summer. The latter result is consistent with previous studies that found that summer sea ice export is not correlated with the monthly averaged atmospheric wind forcing (e.g. Kwok et al., 2004, Wu et al., 2006 and 2007).

The monthly SLP regression map shows some projection onto the NAO centers of action in winter, although the regression values are not statistically significant (Figure 10, middle panel) and of opposite sign to those observed in daily regression maps (Figure 8). To clarify the role of the NAO in forcing sea ice motion on monthly and longer timescales, we removed the leading EOF from the monthly SLP dataset and recomputed the simultaneous regressions on the monthly sea ice index. The leading EOF of the monthly SLP anomalies (Figure 11) resembles the NAO in both winter and summer, and is also similar to the leading EOF of daily SLP anomalies (Figure 2a). With the removal of the leading EOF, the monthly regression map based on year-round data (Figure 12, top panel) is very similar to the daily regression map (Figure 4), with both the Barents and Greenland centers of action present. The amplitude of the SLP dipole is slightly weaker than that based on daily data, but it is still significant at the 99% level.

Similar results are found for winter (Figure 12, middle panel), with both centers of the east-west SLP dipole significant at the 99% level. However, the Barents center of action in winter is noticeably weaker when the leading EOF is removed than when it is included (compare Figures 10 and 12, middle panels). This can be partially attributed to the fact that the Barents region is included in the polar center of action of the leading EOF in winter (Figure 11, middle panel) and thus contributes to the SLP gradient across Fram Strait. In summer (Figure 12, bottom panel) there is no significant relationship between monthly EOF-residual SLP and Fram Strait sea ice motion. The leading EOF in summer is shifted northward compared to that in winter (Figure 11, bottom panel). The lack of relationship between monthly SLP anomalies and Fram Strait sea ice motion in summer (Figures 10 and 12, bottom panels) suggests that high-frequency (e.g. sub-monthly) atmospheric variability plays a dominant role in forcing sea ice motion in summer (Figure 4, bottom panel).

4. Summary

With the help of daily data for SLP and sea ice motion, we found that an east-west dipole pattern with Barents and Greenland centers of action is the most prominent atmospheric driver of sea ice through Fram Strait. The dipole pattern persists year-round, being slightly stronger in winter than in summer. The strongest relationship between the SLP dipole pattern and Fram Strait sea ice motion is simultaneous, with an e-folding time of ~5 days. Spectral analysis shows maximum coherence values in the

10-60 day band. Such a time scale suggests that both high- and low-frequency atmospheric patterns are essential in driving sea ice out of the Arctic.

Repeating our analysis using monthly data revealed a modified spatial pattern of SLP anomalies associated with Fram Strait sea ice motion. While the Barents center of action remains prominent, the Greenland center of action and therefore the dipole structure of the pattern disappeared. However, removing the leading EOF from the monthly-averaged SLP data (e.g. the NAO) resulted in the return of the east-west dipole pattern. Based on these results, we argue that in monthly data the NAO – the leading intrinsic pattern of atmosphere variability – partially masks the relationship between the SLP dipole pattern and the Fram Strait sea ice motion response. That is, the NAO is not the most dynamically relevant pattern for explaining the variations in sea ice motion through Fram Strait. Rather, the east-west SLP dipole pattern is the important driver of the anomalous sea ice motion both in daily and monthly averaged data. These results help explain why previous studies based on monthly data (e.g. Hilmer and Jung, 2000; Vinje 2001, Kwok et al. 2004) found no consistent relationship between the NAO and Fram Strait sea ice motion.

This study investigated the role of atmospheric forcing in driving Fram Strait sea ice motion. To what extent our results may be relevant for sea ice *volume* export remains to be studied. Ice volume changes in the Arctic sea ice are crucial for determining the future behavior of sea ice extent and important for linking the thermodynamic and dynamic components of sea ice change (Holland et al., 2008). As Rigor and Wallace (2004) have argued, the loss of sea ice extent in recent years was preconditioned by the loss of older and thicker sea ice through Fram Strait in the 1990s.

We plan to examine the relationship between atmospheric circulation variability and the sea ice volume flux through Fram Strait by incorporating sea ice thickness data into our analysis.

Acknowledgements. We thank Christophe Cassou for helpful suggestions, Adam Philips and Dennis Shea for technical assistance in preparation of the figures. This work was supported by a grant from the National Science Foundation Arctic System Science Program. The National Center of Atmospheric Research is sponsored by the National Science Foundation.

5. References

1. Bloomfield, 1976. Fourier analysis of time series: an introduction, John Wiley and Sons, pp. 151-181

2. Brummer B, Muller G, Affeld B, Gerdes R, Karcher M, Kauker F, 2001. Cyclones over Fram Strait: impact on sea ice and variability. *Polar Research* 20 (2): 147-152

3. Brummer, B., Muller, G., Hoeber, H., 2003. A Fram Strait cyclone: Properties and impact on ice drift as measured by aircraft and buoys, *J. Geophys. Res*., 108, 4217-4230, DOI: 101029/2002JD002638.

4. Dickson, R.R., Meincke J., Malmberg, S.A. and Lee A.J. 1988. The “Great Salinity Anomaly” in the northern North Atlantic, 1968-1982. *Progr. Oceanogr.* 20”103-151.

5. Duchon C.1979; Lanczos Filtering in One and Two Dimensions, J. Applied Meteorology, 1016-1022

6. Fowler, C. 2003. *Polar Pathfinder Daily 25 km EASE-Grid Sea Ice Motion Vectors*. Boulder, CO, USA: National Snow and Ice Data Center. Digital media.

7. Hilmer, M and T. Jung 2000. Evidence for a recent change in the link between the North Atlantic Oscillation and Arctic sea ice export, *Geophys. Res. Lett*. 27, 989-992

8. Holland, M.M., M.C. Serreze, and J. Stroeve, 2008: The sea ice mass budget of the Arctic and its future change as simulated by coupled climate models, *Clim. Dyn.*, doi:10.1007/s00382-008-0493-4.

9. Hurrell, J.W. 1995. Decadal trends in the North Atlantic Oscillation: regional temperatures and precipitation. *Science* 269: 676-679.

10. Julian P.R. 1975. Comments on the Determination of Significance Levels of the Coherence Statistic. *J. Atmos. Sci*, 32: 836-837.

11. Jung, T and Hilmer M. 2001. The Link between the North Atlantic Oscillation and Arctic sea ice export through Fram Strait. *J. Clim*. 14: 3932-3943.

12. Kalnay, E., M. Kanamitsu, R. Kistler, W. Collins, D. Deaven, L. Gandin, M. Iredell, S. Saha, G. White, J. Woolen, Y. Zhu, M. Chelliah, W. Ebisuzaki, W. Higgens, J. Janowiak, K.C. Mo, C. Ropelewski, J. Wang, A. Leetma, R. Reynolds, R. Jenne, and D. Joseph, 1996, The NCEP/NCAR 40-year reanalysis project, *Bull. Amer. Meteorol. Soc., 77*, 437-471.

13. Kimura, N., and M. Wakatsuchi (2000), Relationship between Sea-Ice Motion and Geostrophic Wind in the Northern Hemisphere, Geophys. Res. Lett., 27(22), 3735-3738.

14. Kolstad, E, Bracegirdle, T.J. and Seierstad I.A 2008. Marine cold-air outbreaks in the North Atlantic: temporal distribution and associations with large-scale atmospheric circulation, *Clim Dyn.* DOI: 10.1007/s00382-008-0431-5

15. Kwok R, Cunningham GF, Pang SS 2004. Fram Strait sea ice outflow. J. Geophys. Res. Oceans, 109 (C1): Art. No. C01009

16. Kwok, R. and Rothrock, D.A., 1999. Variability of Fram Strait ice flux and North Atlantic Oscillation, *J. Geophys. Res. 104(C3),* 5177-5189.

17. Maslanik J., S. Drobot, C. Fowler, W. Emery, R. Barry, 2007. On the Arctic climate paradox and the continuing role of atmospheric circulation in affecting sea ice conditions, Geophys. Res. Lett., 34, L03711, doi:10.1029/2006GL028269.

18. Press. W.H., Flannery, B.P., Teukolsky, S.A., Vetterling, W.T. 1986. Numerical Recipes. The Art of Scientific Computing. Cambridge University Press, pp. 484-488

19. Rigor, I.G. and Wallace, J.M., 2004. Variations in the Age of Arctic sea-ice and summer sea-ice extent. *Geophys. Res. Lett., 31,* L09401, DOI:10.1029/2004GL019492

20. Rigor, I.G.., Wallace, J.M. And Colony, R.L. 2002. Response of sea ice to the Arctic Oscillation, *J. Climate, 15,* 2648-2663.

21. Rogers JC, Yang L, Li L, 2005. The role of Fram Strait winter cyclones on sea ice flux and on Spitsbergen air temperatures, Geophys. Res. Let., 32 (6): Art. No. L06709

22. Skeie, P. 2000. Meridional flow variability over the Nordic seas in the Arctic Oscillation framework, *Geophys. Res. Lett*., 87, 5845-5852

23. Thompson, D.W. and Wallace J.M., 1998. The Arctic Oscillation signature in the wintertime geopotential height and temperature fields. Geophys. Res. Lett. 25: 1297-1300.

24. Thorndike A. S., and R. Colony, 1982: Sea ice motion in response to geostrophic winds. J. Geophys. Res., 87, 5845–5852.

25. Tremblay, B. 2001. Can we consider the Arctic Oscillation independently from the Barents Oscillation? Geophys. Res. Lett, 28: 4227-4230.

26. Tsukernik, M. 2007 Characteristics of the winter cyclone activity in the northern North Atlantic and its impact on the Arctic freshwater budget. PhD Thesis, University of Colorado, 153pp.

27. Vinje, T. 2001. Fram Strait ice fluxes and atmospheric circulation: 1950-2000. *J. Climate, 14,* 3508-3517.

28. Wu, B and M.A. Johnson. 2007. A seesaw structure in SLP anomalies between the Beaufort Sea and the Barents Sea, *Geophys. Res. Lett*., 31, doi: 101029/2006GL028333.

29. Wu, B., J. Wang, and J. Walsh 2006. Dipole anomaly in the winter Arctic atmosphere and its association with sea ice motion, *J. Clim*., 19: 210-225.

6. Figure Captions

Figure 1. Simultaneous correlation map between daily SLP anomalies and daily sea ice motion through Fram Strait during 1979-2006. White contours indicate the 99% significance levels. Fram Strait is outlined by the open red box. Black square boxes show the areas used in SLP gradient index calculation.

Figure 2. 1st and 2nd EOF(s) of Atlantic sector (45 – 90°N, 90°W - 90°E) daily SLP anomalies during 1979-2006. The patterns north of 40°N are obtained by regressing the daily SLP anomalies at all grid point upon the PC time series.

Figure 3. Time series of the standardized daily sea ice motion index through Fram Strait (dashed) and the SLPGI (solid) during the 1985-1986 winter season. The correlation coefficient between the two indices is 0.54.

Figure 4. Simultaneous regression of daily SLP anomalies upon daily anomalies of sea ice motion through Fram Strait based on the period 1979-2006. The top, middle and bottom panels are based on all days of the year, winters (October 15 through April 14) and summers (April 15 to October 14) respectively. White contours indicate the 99% significance levels.

Figure 5. Lead/lag correlation (top) and regression (bottom) coefficients between the daily SLPGI and daily Fram Strait sea ice motion during 1979-2006. Black line represents all days of the year, blue line represents winter (October 15 through April 14) and red line represents summer (April 15 to October 14). Dashed grey lines show the 99% significance levels. Green line in bottom panel shows the lead/lag regression between an NAO-like index (see text for details) and sea ice motion through Fram Strait in winter.

Figure 6. Coherence between the SLPGI and Fram Strait ice motion index based on the daily anomalies during 1979-2006. Dashed grey line indicates the 99% significance value. Highest coherence values (>0.6) are observed in the 10-60 day band, outlined by dotted black lines.

Figure 7. Coherence values between the SLPGI and Fram Strait ice motion index, calculated by averaging the power spectra for each year separately. Black line represents all days of the year, blue line represents winter (October 15 through April 14) and red line represents summer (April 15 to October 14). Note that this method yields higher coherence values for shorter periods (> 5 days) than that in Figure 6. Due to discontinuity from year to year both winter and summer records extend to 180 days only, while year-round values extend to 365 days.

Figure 8. Regression of daily SLP anomalies upon daily anomalies of sea ice motion through Fram Strait based on 10-60 day band pass filtered data for the winter season (October 15 through April 14). Panels represent time evolution of the regression coefficients: from SLP leading sea ice motion by 8 days (-8 day lag) to SLP lagging ice motion by 8 days (+8 day lag). White contours represent the 99% significance levels.

Figure 9. Lead/lag correlation (top) and regression (bottom) coefficients between the daily SLPGI and daily Fram Strait sea ice motion based on 10-60 day band-pass filtered data for 1979-2006. Black line represents all days of the year, blue line represents winter (October 15 through April 14) and red line represents summer (April 15 to October 14). Dashed grey lines show the 99% significance levels. Green line in bottom panel shows the lead/lag regression between an NAO-like index (see text for details) and sea ice motion through Fram Strait in winter.

Figure 10. Simultaneous regression of monthly SLP anomalies upon monthly anomalies of sea ice motion through Fram Strait based on the period of 1979-2006. The top, middle and bottom panels are based on all months of the year, winters (October through March) and summers (April through September) respectively. White contours indicate the 99% significance levels.

Figure 11. The leading EOF of Atlantic sector (45 – 90°N, 90°W - 90°E) monthly SLP anomalies during 1979-2006. The top, middle and bottom panels are based on all months of the year, winters (October through March) and summers (April through September) respectively. The patterns north of 40°N are obtained by regressing the daily SLP anomalies at all grid point upon the PC time series.

Figure 12. As in Figure 10, but the leading EOF of monthly SLP anomalies is removed from the data before the SLP regressions are computed. The top, middle and bottom panels are based on all months of the year, winters (October through March) and summers (April through September) respectively. The leading EOFs for year-round, winter and summer seasons are computed separately. White contours indicate the 99% significance levels.

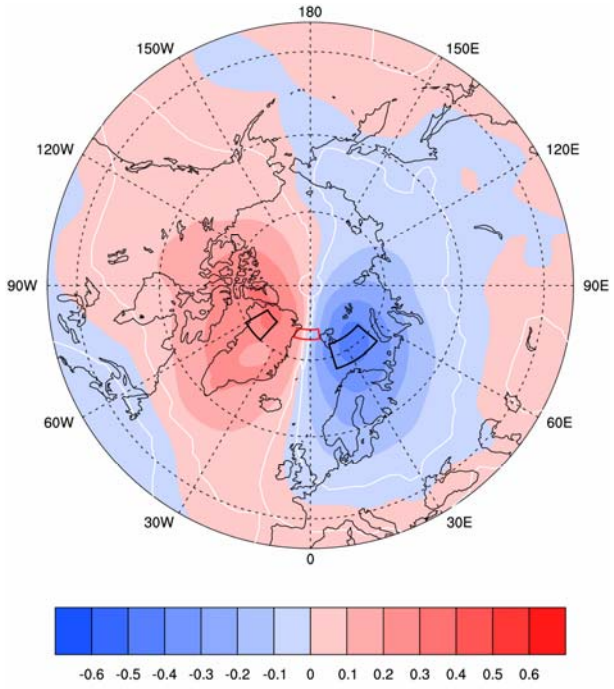

Figure 1. Simultaneous correlation map between daily SLP anomalies and daily sea ice motion through Fram Strait during 1979-2006. White contours indicate the 99% significance levels. Fram Strait is outlined by the red box. Black square boxes show the areas used in SLP gradient index calculation.

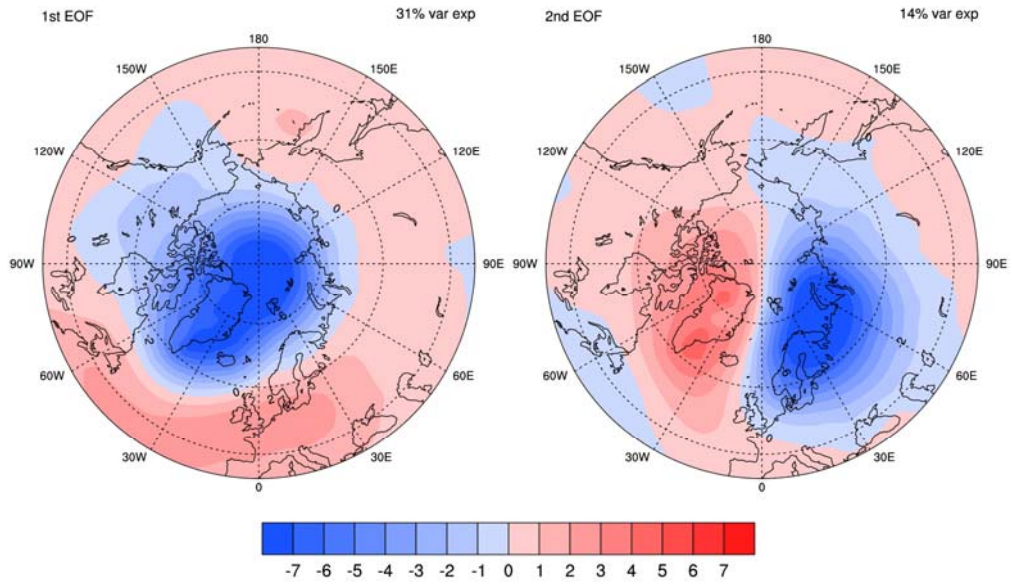

Figure 2. 1st and 2nd EOF(s) of Atlantic sector (45 – 90°N, 90°W - 90°E) daily SLP anomalies during 1979-2006. The patterns north of 40°N are obtained by regressing the daily SLP anomalies at all grid point upon the PC time series.

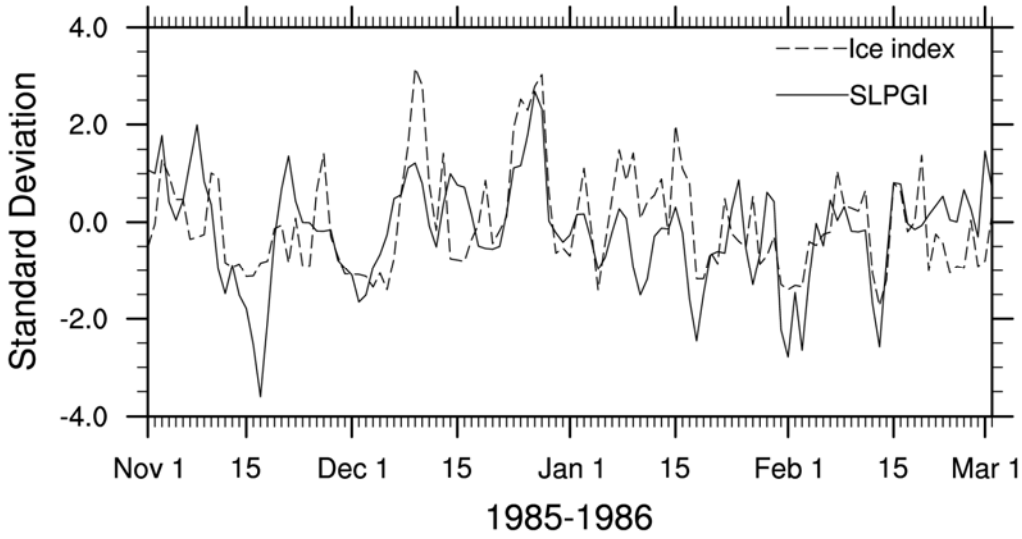

Figure 3. Time series of the standardized daily sea ice motion index through Fram Strait (dashed) and the SLPGI (solid) during the 1985-1986 winter season. The correlation coefficient between the two indices is 0.54.

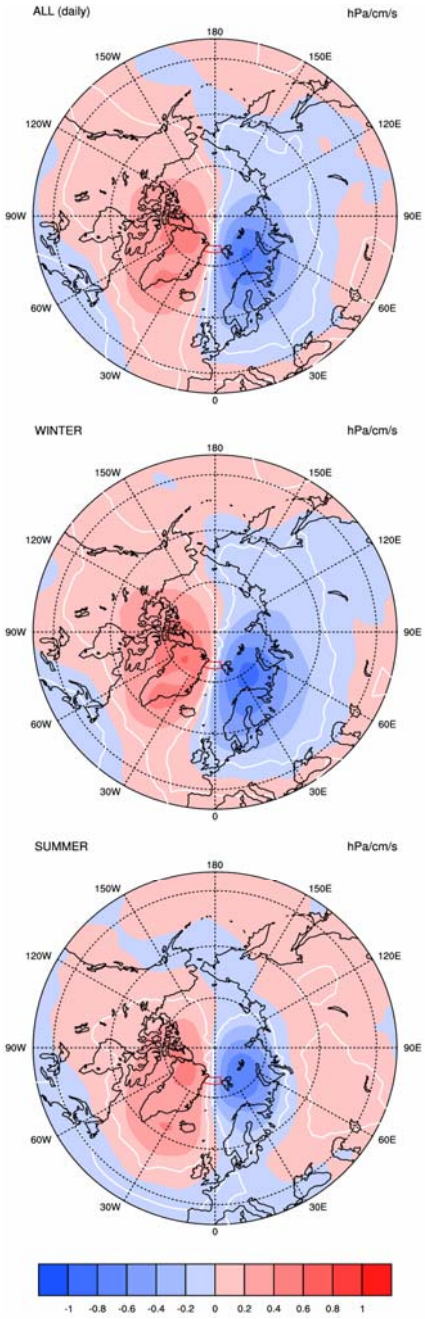

Figure 4. Simultaneous regression of daily SLP anomalies upon daily anomalies of sea ice motion through Fram Strait based on the period 1979-2006. The top, middle and bottom panels are based on all days of the year, winters (October 15 through April 14) and summers (April 15 to October 14) respectively. White contours indicate the 99% significance levels.

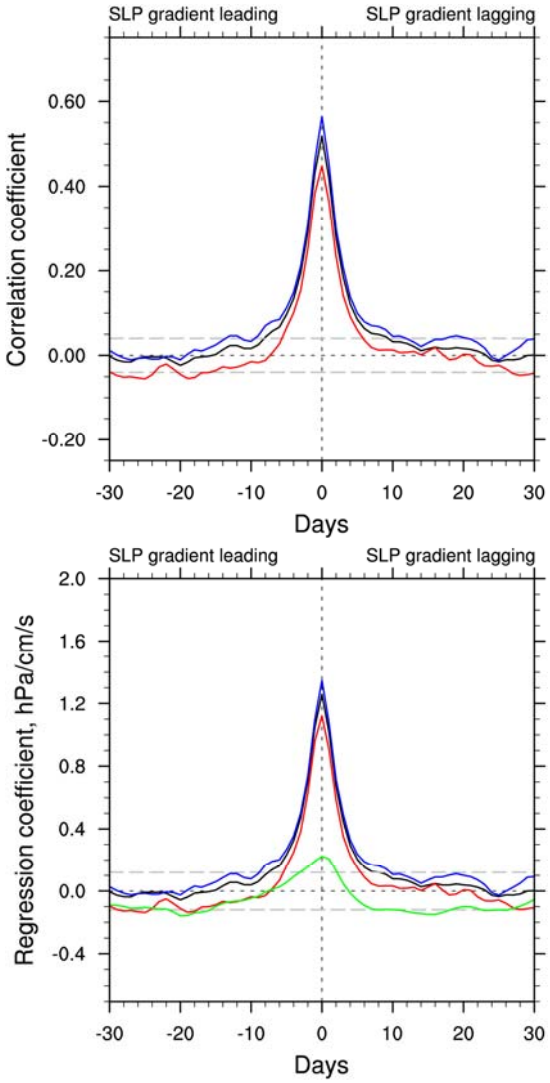

Figure 5. Lead/lag correlation (top) and regression (bottom) coefficients between the daily SLPGI and daily Fram Strait sea ice motion during 1979-2006. Black line represents all days of the year, blue line represents winter (October 15 through April 14) and red line represents summer (April 15 to October 14). Dashed grey lines show the 99% significance levels. Green line in bottom panel shows the lead/lag regression between an NAO-like index (see text for details) and sea ice motion through Fram Strait in winter.

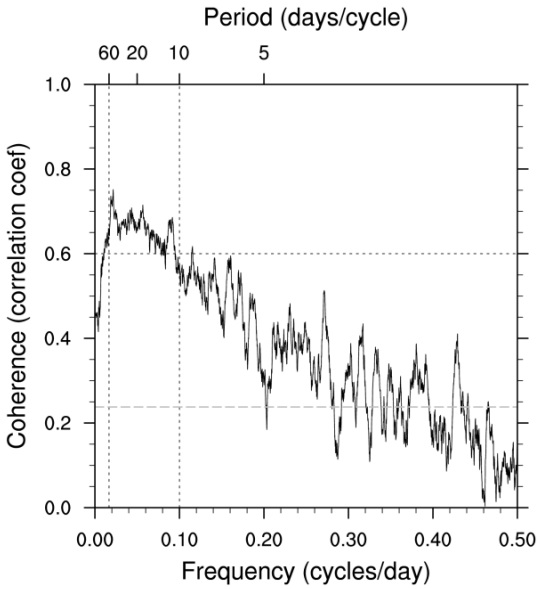

Figure 6. Coherence between the SLPGI and Fram Strait ice motion index based on daily anomalies during 1979-2006. Dashed grey line indicates the 99% significance value. Highest coherence values (>0.6) are observed in the 10-60 day band, outlined by dotted black lines.

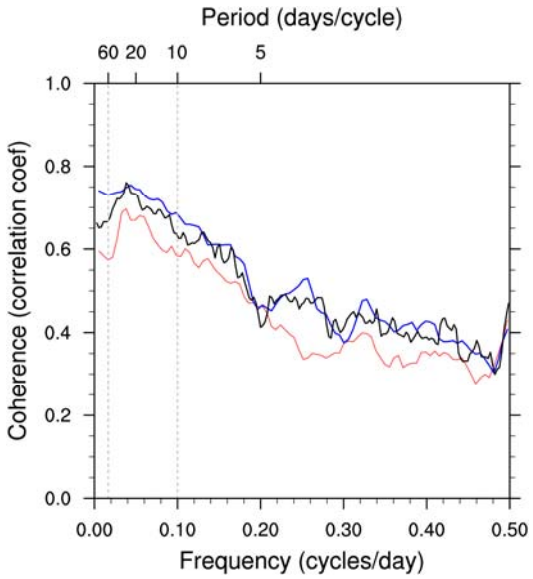

Figure 7. Coherence values between the SLPGI and Fram Strait ice motion index, calculated by averaging the power spectra for each year separately. Black line represents all days of the year, blue line represents winter (October 15 through April 14) and red line represents summer (April 15 to October 14). Note that this method yields higher coherence values for shorter periods (> 5 days) than that in Figure 6. Due to discontinuity from year to year both winter and summer records extend to 180 days only, while year-round values extend to 365 days.

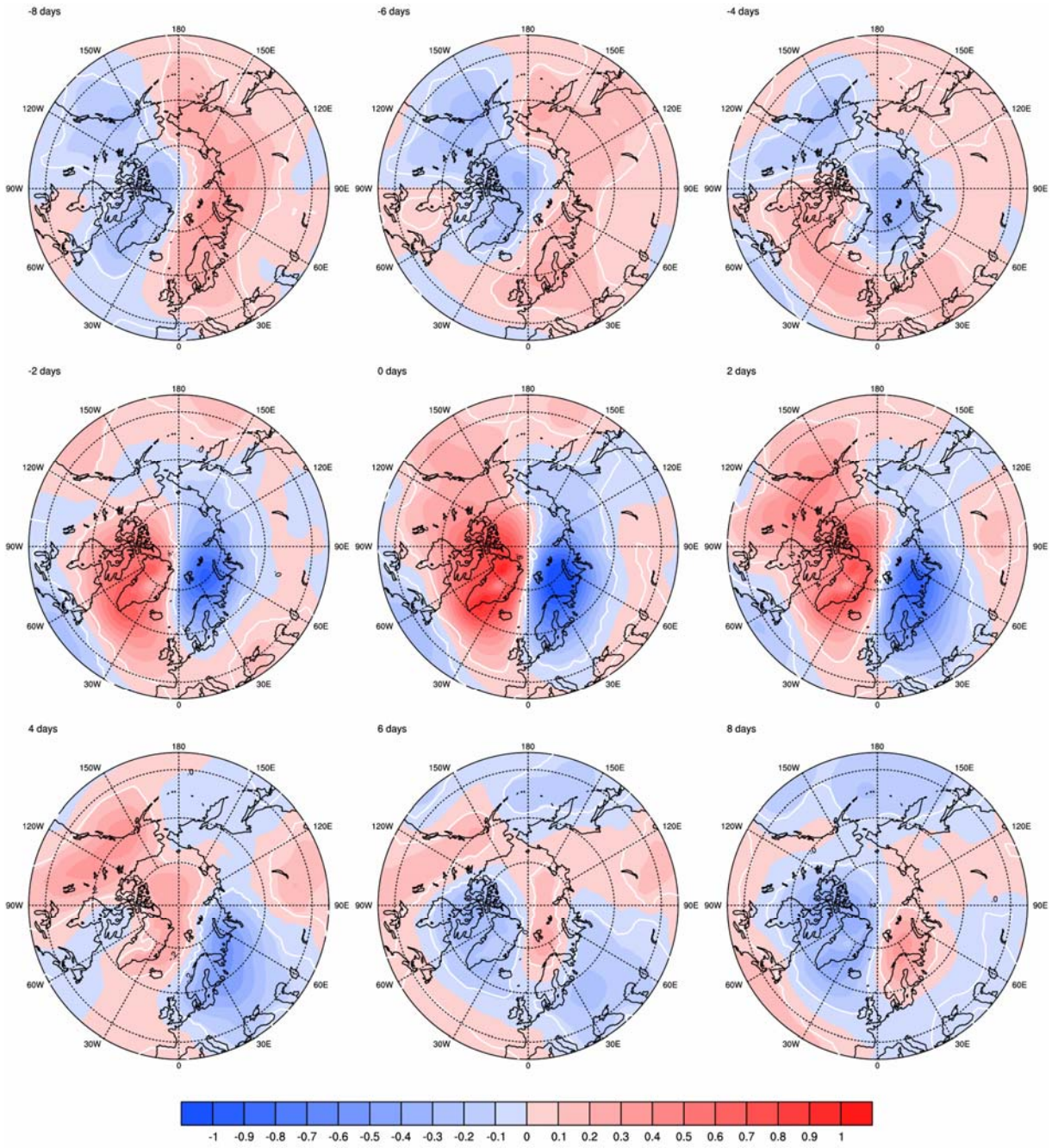

Figure 8. Regression of daily SLP anomalies upon daily anomalies of sea ice motion through Fram Strait based on 10-60 day band pass filtered data for the winter season (October 15 through April 14). Panels represent time evolution of the regression coefficients: from SLP leading sea ice motion by 8 days (-8 day lag) to SLP lagging ice motion by 8 days (+8 day lag). White contours represent the 99% significance levels.

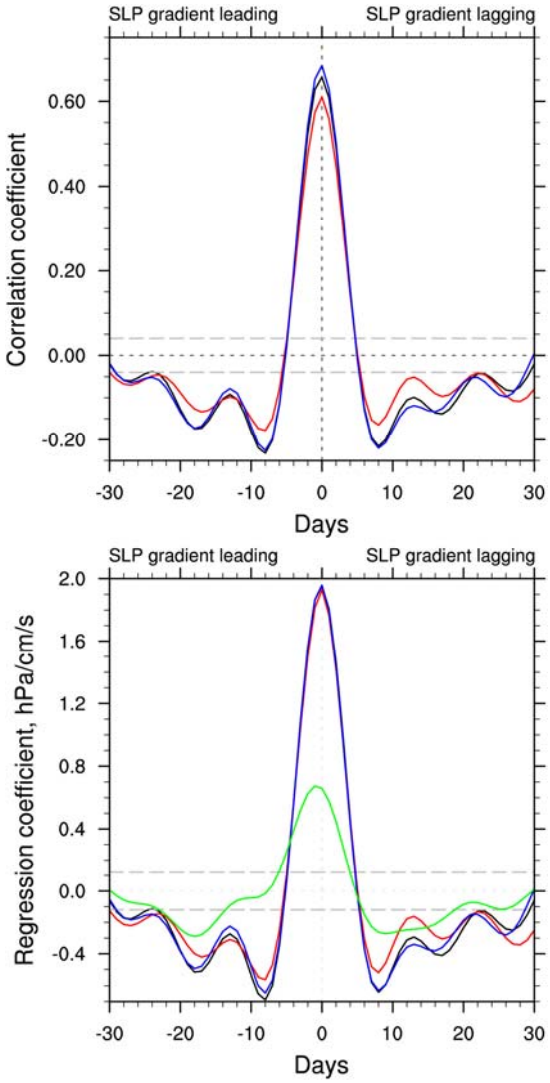

Figure 9. Lead/lag correlation (top) and regression (bottom) coefficients between the daily SLPGI and daily Fram Strait sea ice motion based on 10-60 day band-pass filtered data for 1979-2006. Black line represents all days of the year, blue line represents winter (October 15 through April 14) and red line represents summer (April 15 to October 14). Dashed grey lines show the 99% significance levels. Green line in bottom panel shows the lead/lag regression between an NAO-like index (see text for details) and sea ice motion through Fram Strait in winter.

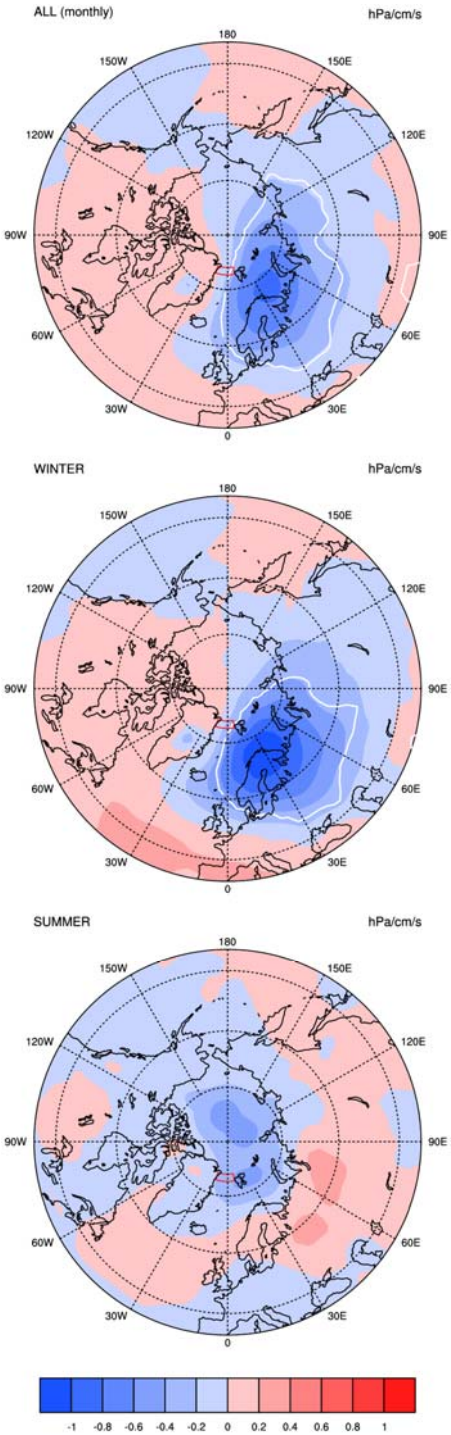

Figure 10. Simultaneous regression of monthly SLP anomalies upon monthly anomalies of sea ice motion through Fram Strait based on the period of 1979-2006. The top, middle and bottom panels are based on all months of the year, winters (October through March) and summers (April through September) respectively. White contours indicate the 99% significance levels.

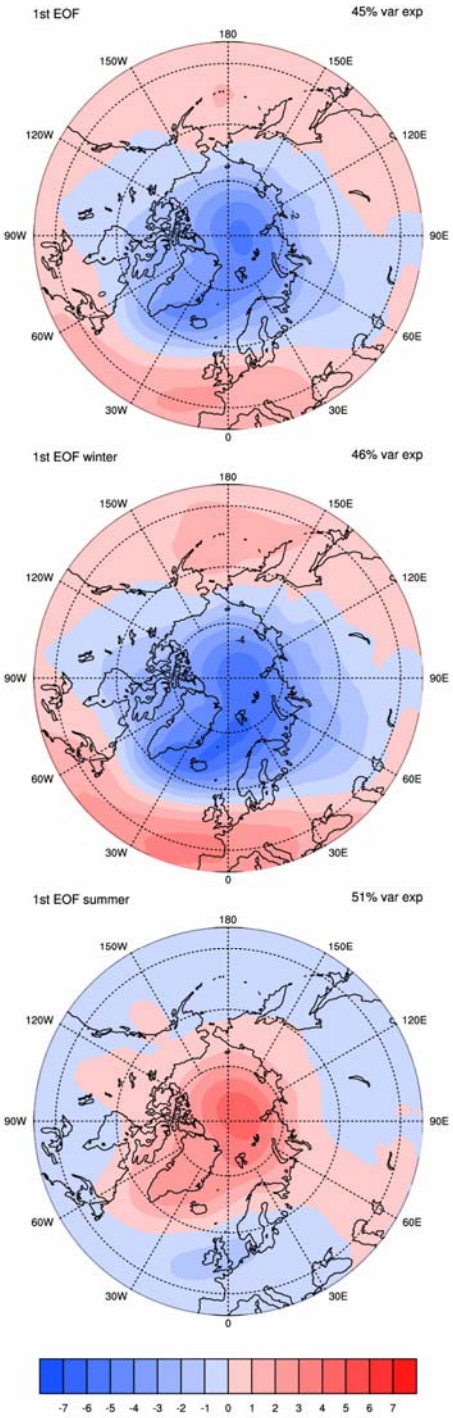

Figure 11. The leading EOF of Atlantic sector (45 – 90°N, 90°W - 90°E) monthly SLP anomalies during 1979-2006. The top, middle and bottom panels are based on all months of the year, winters (October through March) and summers (April through September) respectively. The patterns north of 40°N are obtained by regressing the daily SLP anomalies at all grid point upon the PC time series.

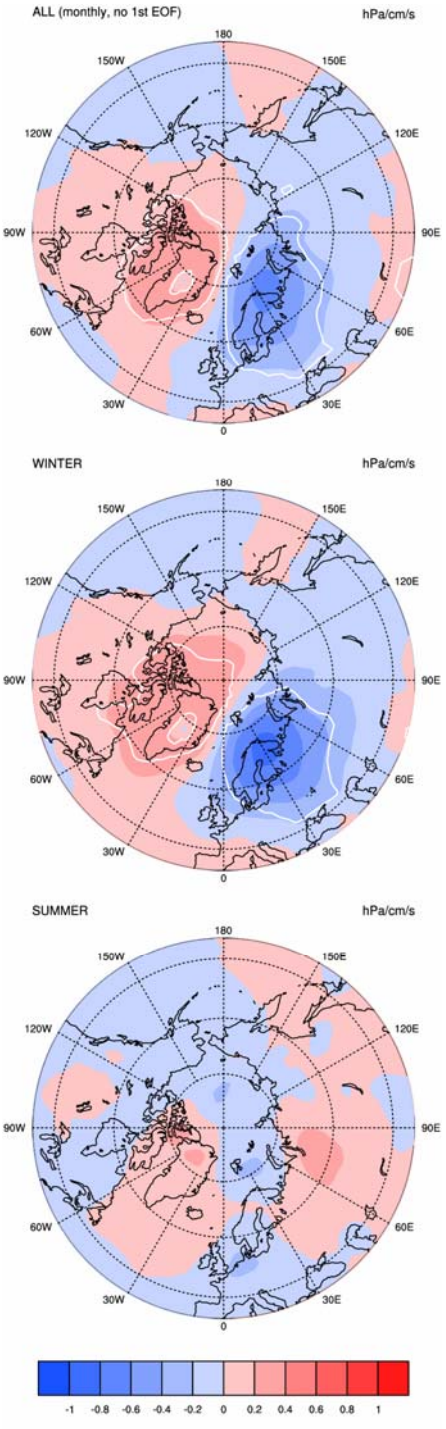

Figure 12. As in Figure 10, but the leading EOF of monthly SLP anomalies is removed from the data before the SLP regressions are computed. The top, middle and bottom panels are based on all months of the year, winters (October through March) and summers (April through September) respectively. The leading EOFs for year-round, winter and summer seasons are computed separately. White contours indicate the 99% significance levels.